Iterative reconstruction algorithm for optoacoustic imaging

G. Paltauf,[a] J. A. Viator, S. A. Prahl, and S. L. Jacques
Oregon Medical Laser Center and Oregon Graduate Institute, Portland, Oregon

(Received 30 October 2000; revised 18 June 2002; accepted 25 June 2002)

Optoacoustic imaging is based on the generation of thermoelastic stress waves by heating an object in an optically heterogeneous medium with a short laser pulse. The stress waves contain information about the distribution of structures with preferential optical absorption. Detection of the waves with an array of broadband ultrasound detectors at the surface of the medium and applying a backprojection algorithm is used to create a map of absorbed energy inside the medium. With conventional reconstruction methods a large number of detector elements and filtering of the signals are necessary to reduce backprojection artifacts. As an alternative this study proposes an iterative procedure. The algorithm is designed to minimize the error between measured signals and signals calculated from the reconstructed image. In experiments using broadband optical ultrasound detectors and in simulations the algorithm was used to obtain three-dimensional images of multiple optoacoustic sources. With signals from a planar array of 3×3 detector elements a significant improvement was observed after about 10 iterations compared to the simple radial backprojection. Compared to conventional methods using filtered backprojection, the iterative method is computationally more intensive but requires less time and instrumentation for signal acquisition.
 [DOI: 10.1121/1.1501898]

PACS numbers: 43.60.Pt, 43.60.Rw, 43.35.Ud [JCB]

I. INTRODUCTION

Optoacoustic or thermoacoustic imaging is a method to localize objects inside an acoustically homogeneous medium that have contrast in the visible, infrared, or microwave range of thee electromagnetic spectrum. It is based on the generation of thermoelastic stress waves as a short pulse from a laser or a microwave source is absorbed by an object in the medium. The contrast for image formation is provided by enhanced heat and stress generation in structures with preferential optical absorption. Compared to conventional ultrasonic pulse-echo imaging, where ultrasound is generated outside the sample and is scattered by acoustical heterogeneities, in optoacoustic imaging the source of pressure waves is the observed target itself. The wavelength of optoacoustic waves depends on size and shape of fluctuations in the distribution of absorbed energy, thus producing a broadband acoustic spectrum that extends over the ultrasonic frequency range, from about 0.1 to 100 MHz. The upper limit is given by $1/t_p$, where t_p is the duration of the exciting pulse. Consequently the resolution limit and at the same time the smallest achievable acoustic wavelength are given by $t_p c$, where c is the speed of sound. Structures larger than this limit fulfill the condition of stress confinement, which states that maximum thermoelastic stress is produced if the heating pulse is shorter than the time the mechanical disturbance needs to escape from a target structure of characteristic size d,

$$t_p \ll t_{\mathrm{ac}} = d/c, \tag{1}$$

where t_{ac} is called the acoustic relaxation time. The pressure waves created in the heated regions propagate to the surface where they are detected with high bandwidth transducers. An image reconstruction method is applied to the signals to create a map of the absorbed energy in the medium. The resulting image is generally not a quantitative reconstruction of a physical property of the material. It rather shows the location of optical absorbers in a similar way as in pulse-echo ultrasound, where acoustical scatterers are located. Only under certain circumstances, such as in the imaging of layered materials with negligible optical scattering, the distribution of the optical absorption coefficient can be reconstructed.

Optoacoustic imaging is applicable to nondestructive testing of materials where the interesting structures have low imaging contrasts for conventional methods like pulse-echo ultrasound but at the same time have high contrast for optical radiation. Sufficient penetration of light to the target structures is also a prerequisite. Since many imaging targets in biological tissue meet these requirements, the optoacoustic method is particularly promising for noninvasive medical imaging. Some structures that are barely seen by established imaging methods employing x rays or ultrasound but exhibit a strong contrast for visible or near infrared light are the increased blood concentration due to neovasculature in breast tumors,[1] vascular abnormalities in skin[2] or inflamed cancerous tissue.[3] Due to the strong scattering of light in tissue, optoacoustic waves are excited by diffusely propagating light. Other than in pure optical imaging, where imaging information comes from diffusely backscattered or transmitted light and the resolution is poor (in the range of 1 cm), in optoacoustic imaging the information about the imaged objects is carried by pressure waves, which are much less scattered than light and are therefore capable of producing images with better resolution (in the range of 1 mm or less). Using multiple wavelengths the spectral information of optical imaging can also be obtained with optoacoustic imaging.

[a]Present address: Institut fuer Experimentalphysik, Karl-Franzens-Universitaet Graz, Universitaetsplatz 5, A-8010 Graz, Austria; electronic mail: guenther.paltauf@kfunigraz.ac.at

The techniques used to transform the information contained in the optoacoustic signals into images depends on the complexity of the target structures. Single, static detectors are used for layered samples.[4–7] More complicated structures can be imaged by scanning a focused acoustic transducer together with the optical source along a line on the surface of an object, creating an image of a two-dimensional section perpendicular to the surface.[7,8] Scanning is, however, limited by the available pulse repetition rate of pulsed lasers, which ranges up to about 100 Hz. To record the amount of data needed for three-dimensional imaging therefore requires parallel detection and processing of optoacoustic signals using ultrasonic transducer arrays. An image of the absorbed light distribution is constructed by backprojecting the acoustic signals among all possible source locations. For a single isotropic detector and a point source these locations lie on the surface of a sphere with the detector in the center. Summation of multiple spheres with their centers at different detector positions generates the reconstruction. If the information contained in the signals about the imaged objects is limited these backprojection spheres (or arcs in a two-dimensional section) tend to remain in the reconstruction, creating image artifacts. The main limitations are the finite number of detector elements and the finite solid angle of detection. Large arrays with plane, curved or hemispherical arrangements of up to 4000 detectors[9,10] or detection principles providing spatially continuous, two-dimensional snapshots of the acoustic pressure distribution in a plane[11,12] have therefore been used to maximize the information that is acquired from the optoacoustic sources. To increase the contrast of interesting structures relative to background absorption and to reduce artifacts, usually a filtering of either the acoustic signals prior to backprojection or of the reconstructed image is performed. High-pass filters reduce the slowly changing signal components caused by background absorption.[1] A method derived from the inverse three-dimensional Radon transform uses backprojection of the temporal derivatives of acoustic pressure signals.[13,14] This method creates full three-dimensional images of the source but needs a high number of detector elements. Filtering methods acting on the reconstructed image use thresholding to remove some of the background or spatial frequency-domain filters to reduce high-frequency backprojection artifacts.[1]

In the present work we propose an alternative concept that reduces artifacts even when signals from only a small number of detectors (e.g., form a 3×3 detector array) are available. This technique increases both contrast and resolution of the reconstructed images, thereby obviating the filtering step used by other techniques. The reconstruction algorithm is iterative and was adapted from algebraic image reconstruction techniques and in particular from the simultaneous iterative reconstruction technique that is used in computer tomography in cases where data sets are noisy and incomplete.[15] The method is also closely related to deconvolution techniques commonly used in fields like spectroscopy[16,17] or microscopy.[18] The basic idea is to treat the image reconstruction as an inverse problem and to minimize the error between the measured acoustic signals and the signals that are calculated with a forward model of optoacoustic sound generation from a reconstructed image. Section II describes the algorithm and the models needed for the forward and the inverse problems. A simulation for a known source distribution and a first experimental reconstruction follow.

II. IMAGE RECONSTRUCTION ALGORITHM

The basic problem of image reconstruction is to invert the forward problem of optoacoustic wave generation and detection. Solution of the forward problem yields pressure-time signals at the element positions in the ultrasonic sensor array, given an initial distribution of absorbed energy in the medium. This distribution is created by absorption of a laser pulse and can be regarded as the source of the pressure wave. In the inverse problem the three-dimensional absorbed energy distribution is sought given a set of acoustic signals at the array positions.

Optoacoustic wave generation is described by the solution of the thermoelastic wave equation.[19,20] Since in soft tissues the optical contrast, which determines the optoacoustic sources, is generally much higher than the small variations of acoustic impedance, an acoustically homogeneous medium is assumed. It is advantageous to use the solution for the velocity potential, which is related to the acoustic pressure by

$$p(\mathbf{r},t) = -\rho \frac{\partial \phi(\mathbf{r},t)}{\partial t}, \tag{2}$$

where ϕ is the velocity potential, ρ the density, p the acoustic pressure, and $\mathbf{r}$ the position of the detector. To model the detection process we use a discrete, matrix-based formulation of the problem that uses a retarded Green's function solution of the thermoelastic wave equation.[13,21] The three-dimensional distribution of volumetric energy density $W(\mathbf{r})$ after absorption of a laser pulse is discretized into a grid of size $N_x\times N_y\times N_z$ and described by a vector $\mathbf{W}$ where each element $W_j (j=1\cdots N_x\times N_y\times N_z)$ contains the average value of the energy density within a volume element of size ΔV at position $\mathbf{r}_j$. A second vector $\boldsymbol{\phi}$ contains the values of the velocity potential measured as a function of time at all positions of the sensor array. The number of measured values ϕ_k is given by the number M of temporal samples in the signal of a single detector, times the number L of detectors in the array. The measurement is described by

$$\boldsymbol{\phi} = \mathbf{AW}$$

or

$$\phi_k = \sum_j A_{kj} W_j$$

with

$$A_{kj} = -\frac{\beta}{4\pi\rho C_p}\frac{\Delta V}{\Delta t}\frac{h_{kj}}{R_{kj}} w_{kj}$$
$$R_{kj} = |\mathbf{r}_k - \mathbf{r}_j|, \quad h_{kj} = \begin{cases} 1 & \text{if } |t_k - R_{kj}/c| < \Delta t/2, \\ 0 & \text{else,} \end{cases} \tag{3}$$

where β is the thermal expansion coefficient, C_p the specific heat capacity at constant pressure, and Δt the time step at which velocity potentials are sampled. The point $\mathbf{r}_k$ is the position of the detector at the kth measurement. The factors w_{kj} contain parameters that describe the detection process. A directional sensitivity of the detectors can be modeled by factors w_{kj} that depend on the angle θ_{kj} between the vector $\mathbf{r}_k - \mathbf{r}_j$ and the normal to the detector plane. According to the definition of h_{kj}, all nonzero elements in a row of **A** belong to volume elements whose centers lie within a spherical shell of radius ct_k and width $c\Delta t$ around $\mathbf{r}_k$. The matrix **A** is extremely sparse and can be quite large (e.g., 1.64×10^5 for typical numbers of $N_x=N_y=N_z=40$, $M=256$ and $L=10$), which precludes a direct matrix inversion. Since most of the elements of **A** are zero a compression can be utilized. First **A** is divided into L submatrices that correspond to single detector positions. Each of these submatrices has only $N_x\times N_y \times N_z$ elements unequal to zero, one per column. This results from the fact that the center of each volume element can only lie within one spherical shell. The nonzero elements are stored in a three-dimensional, $N_x\times N_y\times N_z$ matrix. A second auxiliary matrix of the same size stores the value of k (the row number in the original submatrix of **A**) of each element. To perform the matrix multiplication in Eq. (3), elements of equal k are summed with the help of the auxiliary matrix. The number of elements to be stored is therefore reduced by a factor of $M/2$.

To avoid a loss of information in the modeling of the detection process the spatial increments Δx, Δy, Δz and the time interval Δt have to be matched in a way that the average sound propagation time through a volume element, t_{prop}, is not smaller than Δt. Since the latter is usually predetermined by the sampling interval of the recording instrument the spatial increments are chosen using the inequality

$$\Delta t \leqslant t_{\text{prop}} = \frac{\Delta x + \Delta y + \Delta z}{3c}. \tag{4}$$

Some oversampling (using $\Delta t < t_{\text{prop}}$) increases the accuracy of the calculated signals and is sometimes necessary to limit the size of matrix **A**. However, a calculation with $\Delta t < t_{\text{prop}}$ induces noise (shot noise induced by the arrival of waves from individual volume elements) that can be eliminated by convolving $\boldsymbol{\phi}$ with **g**, a vector containing a Gaussian function with an $1/e$ width corresponding to t_{prop},

$$g_i = \frac{2}{t_{\text{prop}}\sqrt{\pi}} \exp[-(2t_i/t_{\text{prop}})^2]. \tag{5}$$

It has been shown previously that the optoacoustic wave emitted from a small spherical source has a pressure profile given by the time derivative of a Gaussian function.[22] **g** can therefore be regarded as the elementary velocity potential signal that is emitted from a volume element. If the laser pulse duration t_p is longer than t_{prop}, accurate modeling of $\boldsymbol{\phi}$ requires the use of a broader Gaussian function for the convolution, which is done by replacing t_{prop} in Eq. (5) by t_p. Although in practice we first calculated the signals using Eq. (3) and then performed the convolution, we assume for the sake of simplicity the convolution to be integrated in matrix **A** and keep the notation $\boldsymbol{\phi}=\mathbf{AW}$ for the signal generation process (to generate a matrix that includes the convolution a Toeplitz matrix generated from **g** could be multiplied with **A**).

A first-order reconstructed image **I** of the source **W** can be obtained by backprojecting the measured signals $\boldsymbol{\phi}$ into the source volume using a matrix **B**,

$$\mathbf{I} = \boldsymbol{\phi}\mathbf{B}$$

or

$$I_j = \sum_k \phi_k B_{kj}. \tag{6}$$

The backprojection matrix **B** is related to **A**. Different ways to define its elements B_{kj} are possible. The following definition conserves energy, making the sum over all elements of the image vector the same as the sum over the source vector,

$$B_{kj} = \frac{A_{kj}}{L\sum_i A_{ki}^2}. \tag{7}$$

In the resulting image, each volume element is assigned the sum of measured velocity potentials to which it contributed, normalized by $L\sum_i A_{ki}^2$ and weighted with A_{kj}. The sum in the denominator of Eq. (7) takes into account the number of volume elements in each spherical shell. This kind of normalization can cause problem in actual measurements because noise is amplified in image elements that lie on truncated shells near the edges of the source volume. We found that the following definition of B_{kj} gave better results with experimental signals:

$$B_{kj} = -h_{kj}R_{kj}u_{kj}. \tag{8}$$

In this definition the $1/R_{kj}$ attenuation of the optoacoustic generation process is compensated and the backprojection of velocity potentials is weighted with factors u_{kj}. For achieving the best signal to noise ratio in the reconstructed image it has been suggested to set $u_{kj}=w_{kj}$.[9] No normalization with the number of elements is used and consequently no energy conservation is obtained. A separate normalization as described in the following is necessary to achieve energy conservation.

In the above-defined projection the velocity potential measured at a certain time t_k at a certain detector position is smeared over all cells on a spherical shell with radius ct_k. For a detector array with L elements, each point in the source volume is imaged by L spherical shells intersecting at the point location. This has an effect similar to smearing the original with a three-dimensional point spread function. With a small number of array elements this function is strongly dependent on the position in the source volume. Simple filtering operations in frequency domain are therefore not applicable for deconvolution of the reconstructed image. It is obvious that the operation in Eq. (6) is not an inversion of the signal generation process described by matrix **A**. Backprojection can, however, be used to generate reconstructions of optoacoustic sources under two conditions: (1) the data set is sufficiently big, containing signals that are measured from many directions around the source, (2) some kind of filtering

of the signals is used prior to backprojection to improve the image. If the data set is not complete the inverse problem can be solved in an iterative process that is related to a method in computer tomography known as simultaneous iterative reconstruction technique.[15] It is also related to the van Cittert algorithm that was originally used to deconvolve spectra with the response function of the spectrometer.[16,17] The basic idea is to use backprojection to create a first-order image from the measurement $\boldsymbol{\phi}$, calculate new signals $\boldsymbol{\phi}^{(1)}$ from the reconstruction by applying signal generation matrix $\mathbf{A}$ on the image vector, and then add the backprojection of the residual $\boldsymbol{\phi}-\boldsymbol{\phi}^{(1)}$ to the image. Subsequent iterations are described by

$$\begin{aligned}\boldsymbol{\phi}^{(n)}&=\mathbf{KAI}^{(n)},\\ \mathbf{I}^{(n+1)}&=\mathbf{I}^{(n)}+(\boldsymbol{\phi}-\boldsymbol{\phi}^{(n)})\mathbf{B}.\end{aligned} \tag{9}$$

Since the reconstructed energy density has to be positive, a non-negativity constraint is imposed on each new estimate. This means that only positive values are kept in the image and negative values are set to zero. $\mathbf{K}$ is a diagonal matrix that contains for each detector position a normalization coefficient that ensures energy conservation. To derive the coefficient K for a single detector element first a relation between the total absorbed energy Q in the source and the measured velocity potential signal [or acoustic pressure signal with Eq. (2)] is obtained from Eq. (3)

$$Q=\Delta V\sum_j W_j=-\frac{4\pi\rho c C_p}{\beta}\Delta t\sum_k t_k\phi_k. \tag{10}$$

To match $\boldsymbol{\phi}^{(n)}$ energetically with $\boldsymbol{\phi}$, K has to be

$$K=\frac{\sum_k t_k\phi_k}{\sum_k t_k\sum_j A_{kj}I_j^{(n)}}. \tag{11}$$

To obtain a correct value for the total energy from relation (10) requires that all $w_{kj}=1$ and that the detectors are absolutely calibrated. However, even if these requirements are not entirely met the normalization coefficient derived in Eq. (11) will render $\boldsymbol{\phi}$ and $\boldsymbol{\phi}^{(n)}$ comparable in size, which is necessary for calculating the residual. It has to be emphasized that due to different responses of detectors in an array or due to other fluctuations in the measurement the coefficient K can have different values for each detector element. K is therefore an important factor in deriving the correct signals from backprojected images. It has been pointed out that the convergence of the van Cittert algorithm requires suppression of noise.[17] We found that the convolution with $\mathbf{g}$ described in Eq. (5) provides sufficient smoothening of signals to avoid the buildup of noise and to keep the solution converging. Tests with insufficient smoothening, using a shorter integration time than t_{prop}, yielded solutions that diverged after several iterations (not shown).

Iterations start by setting $\mathbf{I}^{(0)}=0$, creating a first estimate $\mathbf{I}^{(1)}$ that is the backprojection of the measured velocity potentials. Since ultrasonic detectors usually measure acoustic pressure, the signals are first converted into velocity potentials by integration. The norm of the residual can be used as a quality measure of the reconstruction and to monitor the improvement achieved by the iterations. The error of the velocity potential after the nth iteration is defined as

$$\text{err}_\phi^{(n)}=\sum_k(\phi_k-\phi_k^{(n)})^2. \tag{12}$$

In the following simulations and experiments, the iterations were stopped if the improvement of the error became smaller than 1% of the initial error, that is

$$\frac{\text{err}_\phi^{(n-1)}-\text{err}_\phi^{(n)}}{\text{err}_\phi^{(1)}}<0.01\,. \tag{13}$$

Using the definition in Eq. (8) for the backprojection matrix, the reconstruction algorithm produces a three-dimensional image in arbitrary units. A normalization by the maximum value is useful for displaying sections of the image and for observing the progress of the iterations. It is also possible to create an absolute image $\mathbf{W}^{(n)}$ in units of absorbed energy density using conservation of energy. Since the volume integral over the reconstructed image has to be equal to the total absorbed energy Q, the images have to be multiplied with a normalization factor

$$\mathbf{W}^{(n)}=\frac{Q}{\Delta V\sum_j I_j^{(n)}}\mathbf{I}^{(n)}. \tag{14}$$

In an experiment the value of Q is obtained from measured signals using Eq. (10). In a simulation it is given by the volume integral over the known source distribution.

III. SIMULATION

We simulated the imaging of two spherical sources using a planar array of 3×3 detectors. The detectors were assumed to be omnidirectional and therefore we set all $w_{kj}=1$. This corresponded to the actual experimental conditions that are described in Sec. IV. Instead of using $u_{kj}=w_{kj}$ we used $u_{kj}=\cos\theta_{kj}$ for the directional weights in the backprojection. The resulting overall weight factors $R_{kj}\cos\theta_{kj}$ are equal to the distance to point $\mathbf{r}_j$ from the detector plane. Backprojection spheres therefore do not reach the detector plane, which slightly decreases the lateral resolution but yields a better convergence of the algorithm compared to isotropic backprojection. The energy density distribution in the sources was given by Gaussian functions with an $1/e$ radius of $a=0.2$ mm,

$$W_j=\exp(-(\mathbf{r}_j-\mathbf{r}_c)^2/a^2), \tag{15}$$

where $\mathbf{r}_c$ is the position of the center. The total source cube had a size of $2\times2\times2$ mm^3 and was divided into a grid of $40\times40\times40$ points. The centers of the two sources (hereafter referred to as ''spheres'') were located at the Cartesian coordinates $\mathbf{r}_{c1}=(1.5,1,0.8)$ mm and $\mathbf{r}_{c2}=(0.5,1,1.3)$ mm. The arrangement of spheres and detector array is schematically shown in Fig. 1. Figure 2 shows one of the velocity potential signals $\boldsymbol{\phi}$ calculated from the original source distribution $\mathbf{W}$, the signal $\boldsymbol{\phi}^{(1)}$ calculated from $\mathbf{I}^{(1)}$ and the residual $\boldsymbol{\phi}-\boldsymbol{\phi}^{(1)}$ that is used to generate the improved estimate $\mathbf{I}^{(2)}$.

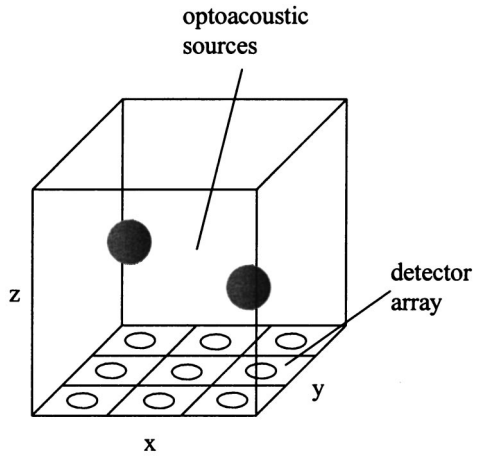

FIG. 1. Geometry of detector array and optoacoustic sources for the simulation.

The resolution of the two sphere signals is diminished in $\boldsymbol{\phi}^{(1)}$, leading to the negative components in the residual. Section images through the centers of the two spheres for the original $\mathbf{W}$, the initial estimate $\mathbf{I}^{(1)}$ and the improved reconstruction after 12 iterations, $\mathbf{I}^{(12)}$ are displayed in Fig. 3. For better comparison of original and reconstruction, all images are normalized by their maximum. The absolute energy density values obtained from Eq. (14) are displayed in the gray level scales. The maximum of $\mathbf{I}^{(1)}$ is only about 5% of the maximum value of $\mathbf{W}$. Furthermore, the source labeled with 1 appears brighter (maximum 0.047) than source 2 (maximum 0.037). The separation of the sources and the accuracy of their relative strengths are clearly improved after 12 iterations. In $\mathbf{I}^{(12)}$ both sources are equally bright with a maximum value of 0.12. Figure 4 displays the error of velocity potentials as a function of the number of iterations. No significant further improvement was achieved after 12 iterations, when the error reached about 40% of its initial value. The fact that the error cannot be further reduced is believed to be due to the small number and plane arrangement of detectors in the array.

The simulation offers the opportunity to quantitatively compare the reconstructed distribution with the known original. This analysis was used to investigate the influence of the

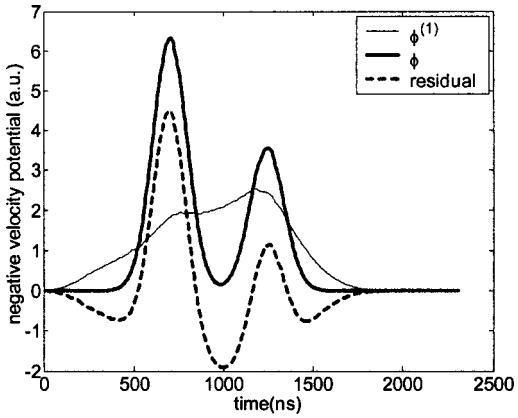

FIG. 2. Simulated velocity potential at one of the nine detector positions. The negative velocity potential is displayed as a function of time. Comparison of the measured signal $\boldsymbol{\phi}$, the signal derived from the first estimate $\boldsymbol{\phi}^{(1)}$ and the residual $\boldsymbol{\phi}-\boldsymbol{\phi}^{(1)}$.

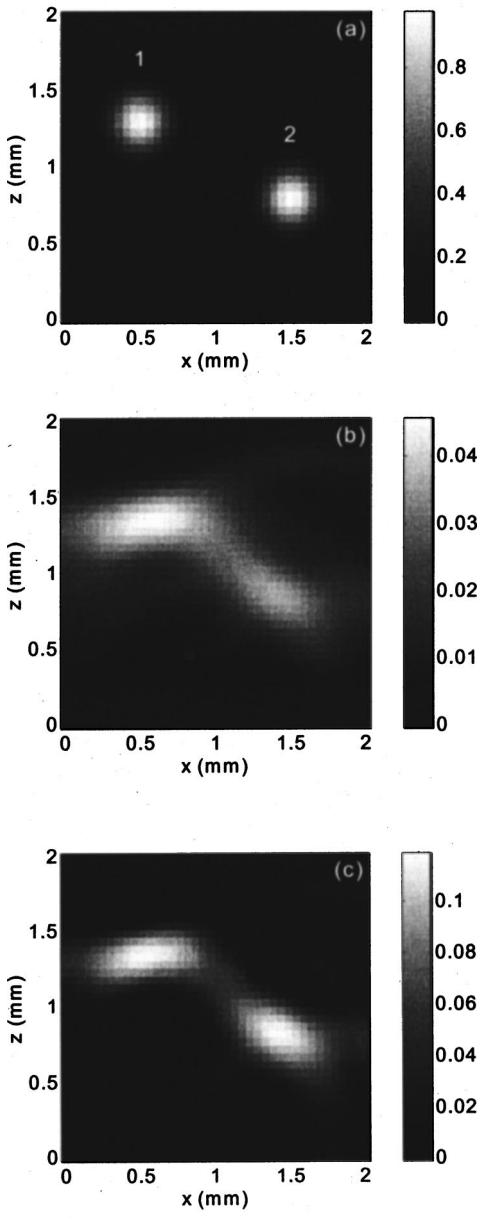

FIG. 3. Simulation of image reconstruction using the iterative algorithm. Displayed is a section through the centers of the spheres at $y=1$ mm. The gray level scales show the values of the reconstruction normalized by the total absorbed energy: (a) original distribution $\mathbf{W}$, (b) first estimate $\mathbf{I}^{(1)}$. Maximum of source 1: 0.047, of source 2: 0.037. (c) Image after 12 iterations $\mathbf{I}^{(12)}$. Maxima of both sources 1 and 2: 0.12.

number of detectors in the array on the quality of the reconstruction. The error of the three-dimensional reconstruction after n iterations can be defined as

$$\mathrm{err}_I^{(n)}=\sum_j (W_j-I_j^{(n)})^2. \tag{16}$$

For a comparison of the shapes of the two distributions, $\mathbf{W}$ and $\mathbf{I}^{(n)}$ are normalized by their maximum value. This corresponds to the visual impression one gets from the section images in Fig. 3, which are normalized in the same way. Alternatively, a comparison of the absolute energy density can be done by replacing $\mathbf{I}^{(n)}$ by $\mathbf{W}^{(n)}$ from Eq. (14). In this simulation, the detectors were always distributed over a square of 2×2 mm^2. The square was divided into a number

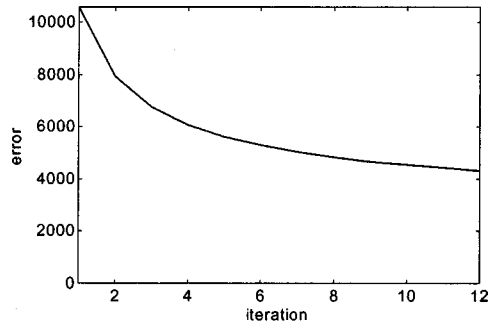

FIG. 4. Errors in the simulation between $\boldsymbol{\phi}$ and $\boldsymbol{\phi}^{(n)}$ as a function of the number of iterations n.

of equal areas according to the number of elements and the detector points were placed in the centers of these areas. Figure 5(a) shows the errors of the reconstruction for the two different normalization methods as a function of the number of array elements. In Fig. 5(b) the mean error of the velocity potential is displayed, also as a function of the number of array elements. The mean error is the value obtained from Eq. (12) divided by the number of array elements, L. All graphs show the final errors after termination of the iterations. Since the radial backprojection is the ideal reconstruction for a single detector, the corresponding error of the velocity potential vanishes. A reconstruction of any three-dimensional object needs at least three detector positions, as indicated by the high errors of the images for 1 and 2 detector elements. The final error of the images decreased until the number of detectors reached 9. There was no significant further improvement when the number of detectors was increased from 9 to 16. The improvement was much more pronounced in the reconstruction that was normalized by its maximum value than in the absolute reconstruction. The final error of the velocity potential was constant for 4, 6, 9, and 16 detector elements. From this analysis it follows that for the reconstruction of simple objects as the two spheres a number of 9 detector elements is sufficient. The use of 16 elements insignificantly improves the reconstruction but almost doubles the computation time.

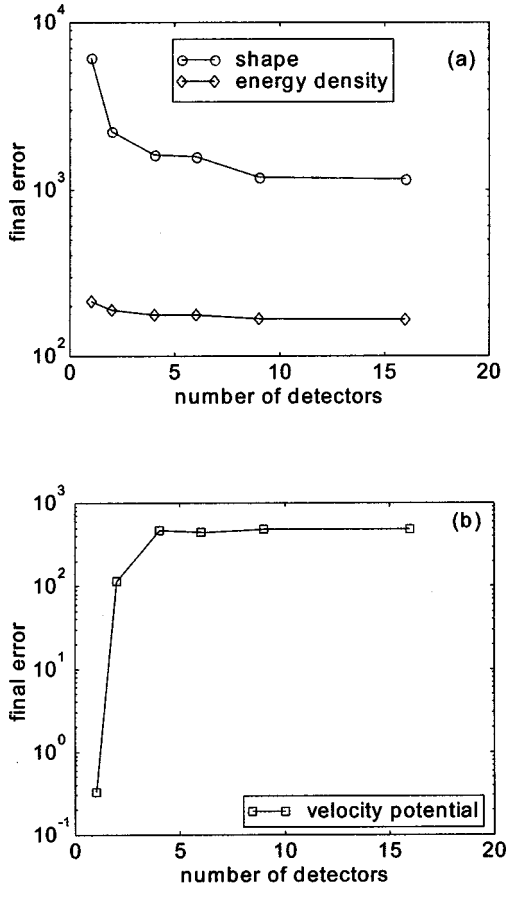

FIG. 5. Final errors in the simulation as a function of the number of detectors in a quadratic array. (a) Error of the reconstructed image. For comparison of shapes both $\mathbf{W}$ and $\mathbf{I}^{(n)}$ are normalized to their maximum. Comparison of energy density is done after normalizing $\mathbf{I}^{(n)}$ using the total absorbed energy. (b) Final error of velocity potential. Errors calculated with Eq. (13) are divided by the number of array elements.

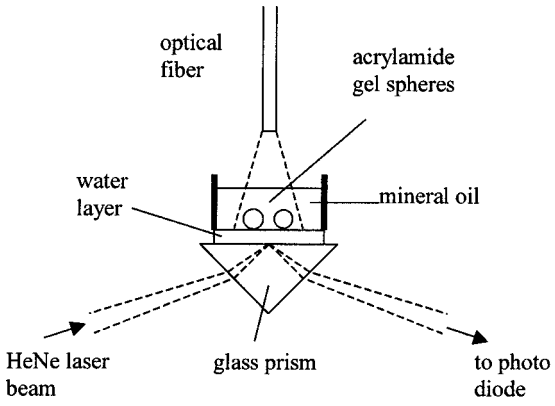

FIG. 6. Experimental setup for the optoacoustic imaging of two absorbing spheres. For detection of the acoustic waves, a focused laser beam is modulated by pressure changes at a glass–water interface.

IV. EXPERIMENT

In an experiment we tested the iterative algorithm for the imaging of two absorbing sources in an optically clear environment. Two spheres made of acrylamide gel with added absorber (Direct Red 81, Sigma Chemical) were placed on a thin plastic film and were surrounded by clear mineral oil (Fig. 6). The absorption coefficient of the gel was $\mu_a = 60\ \mathrm{cm}^{-1}$. The oil prevented the dye from diffusing out of the spheres. The diameters of the spheres were 1.2 and 1.5 mm, respectively, and the distance between the centers was 2.15 mm. A 1-mm-diameter optical fiber was used to irradiate the spheres from above. The laser source was a frequency-doubled, Q-switched Nd:YAG laser operating at a wavelength of 532 nm with a pulse duration of 5 ns. The laser pulse energy was 5 mJ and the laser spot diameter was 4 mm. With an optical absorption depth $1/\mu_a$ of 170 μm both spheres were optically thick, and therefore only a thin layer facing the incident laser pulse was heated. The acoustic signals were recorded with an optical detector described previously.[23] A continuous HeNe probe beam was focused to an elliptical spot with principal diameters of 120 and 250 μm on the interface of a glass prism and a water layer. The layer separated the glass prism from the plastic film carrying the gel spheres and had a thickness of 3 mm. An acoustic wave being incident on the glass surface from the water layer

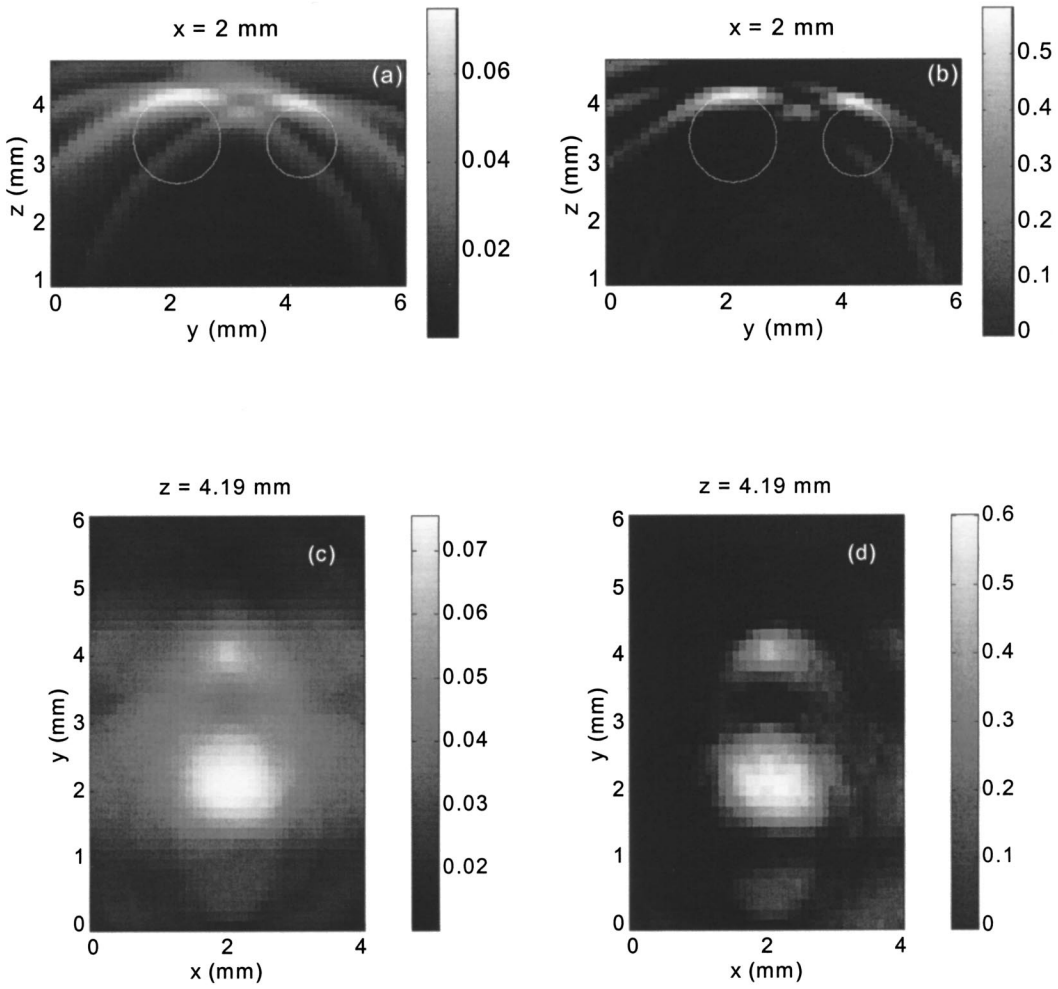

FIG. 7. Experimental image reconstruction. Sections along $y-z$ planes [(a), (b)] and $x-y$ planes [(c), (d)] of the first estimate $\mathbf{I}^{(1)}$ [(a), (c)] and the estimate after 11 iterations, $\mathbf{I}^{(11)}$ [(b), (d)] are displayed. The values of the gray level scales are in J/cm^3. The circles in (a) and (b) indicate the positions of the absorbing spheres.

slightly changed the relative optical refractive index between the two media, thereby varying the Fresnel reflectance of the interface. This caused modulations of the probe beam intensity that were detected with a fast photodiode. The signals from the photodiode were amplified and recorded on a digital storage oscilloscope. Choosing an incident angle of the probe beam slightly smaller than the critical angle of total internal reflection of the glass-water interface maximized the sensitivity of the detector. The undisturbed optical reflectance at the prism–water interface was 0.8. Calibrating the detector using a procedure based on the Fresnel formula and the change of refractive index with pressure, $dn/dp = 1.35 \times 10^{-5}$ bar^{-1} yielded a sensitivity of 0.6% modulation per bar of pressure.[23] The overall sensitivity of the system taking into account the response of the photodiode and the gain of the amplifier was 1 mV/bar. The noise level of averaged signals (over 32 sweeps) was about 20 μV or 20 mbar.

The directivity of an ultrasound detector for pulsed excitation is known to depend on the size of the sensor area, the distance between source and detector and the temporal shape and duration of the signal, which are in turn determined by the shape of the source and the pulse duration of the laser.[9] Unlike a piezoelectric element that is sensitive to the pressure that enters into the piezoelectric material, the optical sensor measures changes of pressures and associated density modulations that occur at the surface of the glass prism. Therefore there is no angle-dependent attenuation of the pressure wave due to acoustic mismatch for the optical sensor and only the integration effect of the obliquely incident wave on the detector plane plays a role. In a separate experiment (not shown) we found that indeed the directional dependence of signal shape and maximum can be readily described by integration effects over the detector area. It turned out that for the experimental signal shapes and within the aperture used for the experiment the optical detector can be regarded as omnidirectional. Consequently we set all weight factors $w_{jk} = 1$, independent of angle. To simulate a detector array, the detector point was scanned over a grid of 3×3 points in a plane, with a grid size of 1 mm in x direction and of 1.5 mm in the y direction.

V. RESULTS

Figure 7 shows two sections of the reconstructed volume (size $4 \times 6 \times 4$ mm^3), one parallel to the $y-z$ plane and one parallel to the $x-y$ plane. The algorithm stopped after 11 iterations. For each plane, the first-order reconstruction, $\mathbf{I}^{(1)}$, and the final reconstructed image, $\mathbf{I}^{(11)}$, are displayed. The

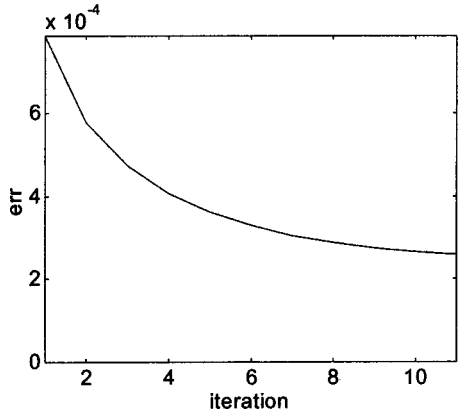

FIG. 8. Experimental image reconstruction: errors between $\boldsymbol{\phi}$ and $\boldsymbol{\phi}^{(n)}$ as a function of the number of iterations n.

$y-z$ section shows how the backprojection arcs are strongly reduced after 11 iterations. In an $x-y$ section, the backprojection artifacts cause a blur that again nearly disappears in the improved image. The values in the gray level bar are absorbed energy density in units of J/cm^3. They were obtained by normalizing $\mathbf{I}^{(n)}$ using Eq. (14). The total absorbed energy was calculated from the measured acoustic signals using Eq. (10), giving an average value of 1.5 mJ. This is a reasonable value considering that the incident laser pulse energy was 5 mJ and that the cross section of the spheres only partly filled the laser spot. From iteration 1 to iteration 11 the maximum energy density increased by a factor of 8, due to the less spreading of energy over the backprojection spheres and increased concentration in the two sources. The corresponding errors are shown in Fig. 8.

VI. DISCUSSION

An iterative method has been described to reconstruct the distribution of absorbed energy density from thermoelastic pressure signals detected with a transducer array. The minimization of the error between the measured signals and the signals calculated from the reconstructed distribution leads to a self-consistent solution of the optoacoustic imaging problem and an inversion of Eq. (3). All knowledge about the source that is required in the algorithm comes from the measured signals and the condition that the result has to be positive.

During the iterations the artifacts, which appear as backprojection arcs or blur in the two-dimensional sections of $\mathbf{I}^{(1)}$, were markedly reduced. Comparing initial estimates with improved estimates in Figs. 3 and 7 might suggest that similar improvements could be achieved by simple thresholding, where parts of the images are set to zero that are darker than a certain threshold. However, the sources may have different strengths, and thresholding could also remove actual structures together with the artifacts. In addition, as the simulation has shown the one-step backprojection sometimes produces incorrect relative source strengths. Applying a threshold to remove backprojection arcs to the reconstruction in Fig. 3(b) would have emphasized this error. Instead the iterative algorithm was able to correct the reconstruction and to make the brightness of the two sources equal.

The maximum of the absolute source strength was always too low compared to the original. In the simulations the maximum reconstructed energy density increased between $\mathbf{I}^{(1)}$ and $\mathbf{I}^{(11)}$ from about 5% to 12% of the corresponding value in the original distribution $\mathbf{W}$. In the experiment, an eightfold increase of maximum energy density from 0.075 to 0.6 J/cm^3 was observed. This was still too low compared to an estimated value of 2.4 J/cm^3 derived from the experimental parameters using

$$W_{\max}=\frac{Q}{A_{\text{las}}}\mu_a, \tag{17}$$

where A_{las} is the laser spot area of 0.126 cm^2, and the values of laser pulse energy Q and absorption coefficient μ_a are 5 mJ and 60 cm^{-1}, respectively. The reason why the algorithm tends to give too low maximum values is the effect of slight spreading of energy around a reconstructed source on the sum in the denominator of Eq. (14). The energy content in residual artifacts increases the integral and reduces the maximum value of the image.

The error in the velocity potential did not approach zero but rather seemed to converge to a certain constant level. This shows the limit of the algorithm when it is applied to data recorded on a finite size plane array. Backprojection of residual terms in Eq. (9) can only correct the reconstruction from a limited range of directions, leaving artifacts that cannot be corrected at all. The algorithm is expected to be more efficient if spheres from all directions intersect in one image point, that is if the detectors are arranged on a spherical array around the imaged volume. In practical applications, however, this is usually not possible. Applying the algorithm to signals from curved arrays with an increased solid angle of detection compared to a plane array should improve the convergence.

Since all information for the reconstruction comes from the measured signals, the detectors have to be very accurate. The main requirements are sufficiently high bandwidth and the absence of measuring artifacts such as ringing. The optical detector used in this study met these requirements. Another advantage of the optical detector is that it is transparent and can be transilluminated by the laser pulse. This makes it easier to apply laser pulses and to collect the acoustic signals on the same surface of a sample. A drawback is that the sensitivity of optical detection using changes of Fresnel reflection is limited to about 1% modulation per bar.[12] For the acoustic pressure amplitudes recorded in our experiments (in the range of 0.2 bar) this yielded a satisfactory signal to noise ratio. However, if higher sensitivity is needed, piezoelectric detectors should be employed and appropriate filtering of signals incorporated to remove measurement artifacts.[10]

In optoacoustic imaging, the reconstruction problem is always three-dimensional.[14] This is partly caused by the diffuse propagation of the light pulse that excites the thermoelastic wave. It is therefore not possible to limit the generation of signals to a plane as in 2D x-ray computer tomography, where information from only a single, thin section of the sample is projected. Reconstruction of a 2D slice therefore requires collection of information from the whole volume to discriminate sources in the imaged section from

those outside this section. Furthermore, knowing only the source distribution in a cross-sectional plane, it is impossible to solve the optoacoustic wave equation to obtain a set of signals. The algorithm developed in this study can therefore only be applied to the full source volume. This makes the method computationally intensive. Generating or backprojecting a signal from or to a volume of $40\times40\times40$ points took about 6 s on a G4 Power PC (Apple Computer, Inc.). Using 9 detector positions, one full iteration was accomplished in a little less than 2 min and the whole reconstruction using 11 iterations required 22 min.

An important question is the performance of the iterative algorithm in comparison with existing methods. Thermoacoustic images with a quality comparable to x-ray CT have been obtained with hemispherical arrays and microwave pulse sources.[10] Pressure signals from an array of 4000 or more elements are differentiated before backprojection, leading to a reconstruction method similar to the inverse three-dimensional Radon transform. Taking the first derivative of pressure (equivalent to the second derivative of velocity potential) leads to signals that have some similarity to the residuals that are used to improve the first image estimate in the iterative algorithm (Fig. 2). Employing the filtered backprojection to our experimental signals we obtained a reconstruction with an error of the velocity potential of 7.4×10^{-4}, which is lower than 7.8×10^{-4} achieved with backprojection of unfiltered signals but higher than the final error of the iterative algorithm of 2.6×10^{-4}. This shows that the inverse Radon method is not designed to work with a low number of detectors, where the feedback provided by the iterative algorithm has the better correcting effect. Another method of filtered backprojection uses a high pass filter to remove the slowly changing signal from background absorption. This creates new pressure and velocity potential signals that correspond only to small structures with contrast relative to the background.[1] A similar kind of filtering could be useful to process the signals that are used as input for the iterative algorithm, which would then produce a corrected image of only these structures.

VII. CONCLUSION

Iterative reconstruction of three-dimensional optoacoustic images leads to a significant reduction of artifacts, a correction of relative source strengths and an improvement of contrast compared to a single backprojection of velocity potentials. Compared to existing reconstruction techniques for three-dimensional optoacoustic or thermoacoustic imaging that use filtered backprojection of signals and high numbers of detector array elements the iterative method uses a low number of elements and a minimization technique that replaces the filtering step. The method may be useful in imaging applications where only a small number of array elements can be used, for example if the time for signal acquisition and the size of the transducer are limited.

Apart from the optoacoustic imaging problem the proposed reconstruction technique could also be applied to other problems in acoustics where the imaged objects are at the same time sources of acoustic waves. In the theoretical description it is shown how the temporally retarded signals from an acoustic source can be calculated using a set of linear equations. The reconstruction method is based on these equations, however, the way in which sound is generated is not limited to the optoacoustic effect.

ACKNOWLEDGMENT

G.P. was supported by the Austrian Program for Advanced Research and Technology (APART) of the Austrian Academy of Sciences.

[1] V. A. Andreev, A. A. Karabutov, S. V. Solomatin, E. V. Savateeva, V. Aleynikov, Y. V. Zhulina, R. D. Fleming, and A. A. Oraevsky, ''Optoacoustic tomography of breast cancer with arc-array-transducer,'' in *Biomedical Optoacoustics*, edited by A. A. Oraevsky [Proc. SPIE **3916**, 36–47 (2000)].

[2] C. G. A. Hoelen, F. F. M. de Mul, R. Pongers, and A. Dekker, ''Three-dimensional photoacoustic imaging of blood vessels in tissue,'' Opt. Lett. **23**, 648–650 (1998).

[3] S. L. Jacques, J. A. Viator, and G. Paltauf, ''Optoacoustic imaging of tissue blanching during photodynamic therapy of esophageal cancer,'' in *Biomedical Optoacoustics*, edited by A. A. Oraevsky [Proc. SPIE **3916**, 322–330 (2000)].

[4] A. A. Oraevsky, S. L. Jacques, R. O. Esenaliev, and F. K. Tittel, ''Laser-based optoacoustic imaging in biological tissues,'' in *Laser-Tissue Interaction V*, edited by S. L. Jacques [Proc. SPIE **2134A**, 122–128 (1994)].

[5] J. A. Viator, S. L. Jacques, and S. A. Prahl, ''Depth profiling of absorbing soft materials using photoacoustic methods,'' IEEE J. Sel. Top. Quantum Electron. **5**, 989–996 (1999).

[6] A. A. Karabutov, N. B. Podymova, and V. S. Letokhov, ''Time-resolved laser optoacoustic tomography of inhomogeneous media,'' Appl. Phys. B: Lasers Opt. **63**, 545–563 (1996).

[7] G. Paltauf and H. Schmidt-Kloiber, ''Pulsed optoacoustic characterization of layered media,'' J. Appl. Phys. **88**, 1624–1631 (2000).

[8] E. V. Savateeva, A. A. Karabutov, M. Motamedi, B. Bell, R. Johnigan, and A. A. Oraevsky, ''Noninvasive detection and staging of oral cancer *in vivo* with confocal opto-acoustic tomography,'' in Ref. 1, pp. 55–66.

[9] C. G. A. Hoelen and F. F. M. de Mul, ''Image reconstruction for photoacoustic scanning of tissue structures,'' Appl. Opt. **39**, 5872–5883 (2000).

[10] R. A. Kruger, D. R. Reinecke, and G. A. Kruger, ''Thermoacoustic computed tomography,'' Med. Phys. **26**, 1832–1837 (1999).

[11] G. Paltauf, H. Schmidt-Kloiber, K. P. Köstli, and M. Frenz, ''Optical method for two-dimensional ultrasonic detection,'' Appl. Phys. Lett. **75**, 1048–1050 (1999).

[12] G. Paltauf, H. Schmidt-Kloiber, K. P. Koestli, M. Frenz, and H. P. Weber, ''Optoacoustic imaging using two-dimensional ultrasonic detection,'' in Ref. 1, pp. 240–248.

[13] P. Liu, ''Image reconstruction from photoacoustic pressure signals,'' in *Laser-Tissue Interaction VII*, edited by S. L. Jacques [Proc. SPIE **2681**, 285–296 (1996)].

[14] P. Liu, ''The P-transform and photoacoustic image reconstruction,'' Phys. Med. Biol. **43**, 667–674 (1998).

[15] A. C. Kak and M. Slaney, *Principles of Computerized Tomographic Imaging* (IEEE Press, New York, 1988).

[16] P. H. van Cittert, ''Zum einfluβ der spaltbreite auf die intensitätsverteilung in spektrallinien'' (Influence of slit width on the intensity distribution in spectral lines), Z. Phys. **69**, 298–308 (1931).

[17] P. A. Jansson, ''Method for determining the response function of a high-resolution infrared spectrometer,'' J. Opt. Soc. Am. **60**, 184–191 (1970).

[18] D. A. Agard, ''Optical sectioning microscopy: Cellular architecture in three dimensions,'' Annu. Rev. Biophys. Bioeng. **13**, 191–219 (1984).

[19] V. E. Gusev and A. A. Karabutov, *Laser Optoacoustics* (American Institute of Physics, New York, 1993).

[20] G. J. Diebold and T. Sun, ''Properties of photoacoustic waves in one, two, and three dimensions,'' Acustica **80**, 339–351 (1994).

[21] G. Paltauf, H. Schmidt-Kloiber, and M. Frenz, ''Photoacoustic waves excited in liquids by fiber-transmitted laser pulses,'' J. Acoust. Soc. Am. **104**, 890–897 (1998).

[22] C. G. A. Hoelen and F. F. M. de Mul, ''A new approach to photoacoustic signal generation,'' J. Acoust. Soc. Am. **106**, 695–706 (1999).

[23] G. Paltauf and H. Schmidt-Kloiber, ''Measurement of laser-induced acoustic waves with a calibrated optical transducer,'' J. Appl. Phys. **82**, 1525–1531 (1997).